Chinese Chemical Letters 37 (2026) 111282

Contents lists available at ScienceDirect

Chinese Chemical Letters

journal homepage: www.elsevier.com/locate/cclet

Overcoming the drug retention barrier with photosensitive hydrogel for sustained photodynamic therapy of oral leukoplakia

Zhengzheng Lv[a], Xin Xia[b], Peisheng Cao[a], Qi Han[c], Hang Zhao[b], Ronghui Zhou[b,*], Peng Wu[a]

[a] Analytical & Testing Center, Sichuan University, Chengdu 610064, China
[b] State Key Laboratory of Oral Diseases, National Clinical Research Center for Oral Diseases, West China Hospital of Stomatology, Sichuan University, Chengdu 610041, China
[c] West China Hospital of Stomatology, Oral Pathology, Sichuan University, Chengdu 610041, China

ARTICLE INFO

Article history:
Received 1 April 2025
Revised 29 April 2025
Accepted 30 April 2025
Available online 30 April 2025

Keywords:
Oral leukoplakia
Photosensitive hydrogel
Graphene quantum dots
Drug retention time
Sustained photodynamic therapy

ABSTRACT

Oral leukoplakia (OLK) is a common and representative malignant disease of oral mucosa, and possess a higher risk of cancer. Compared with traditional surgical treatment, photodynamic therapy (PDT) has great potential in OLK treatment, due to its advantages of minimally invasiveness and low toxic side effects. However, traditional photosensitizer administration suffers from short retention time due to the fluid environment of saliva and extensive tongue movement, leading to poor drug (photosensitizer) utilization and limited therapeutic outcome. To address such issue, here a photosensitive guanosine (G)-based hydrogel system (G@GQD) was constructed, in which graphene quantum dots (GQDs) featuring high photosensitization activity was loaded through three dimensional (3D) fiber network physical encapsulation. The favorable adhesion of the G@GQD hydrogel on the tongue, together with sustained GQDs release, significantly enhanced the retention of GQDs within the oral cavity. As a result, G@GQD hydrogel could continuously generate high levels of reactive oxygen species (ROS) under irradiation, demonstrating a sustained therapeutic efficiency *in vitro*. Compared with free GQDs, G@GQD exhibited significantly improved PDT efficiency in treating 4-nitroquinoline 1-oxide (4-NQO)-induced OLK animals. This study presented a promising strategy in overcoming the drug retention barrier that caused by saliva and tongue movement, which has far-reaching significance for the future PDT therapies.

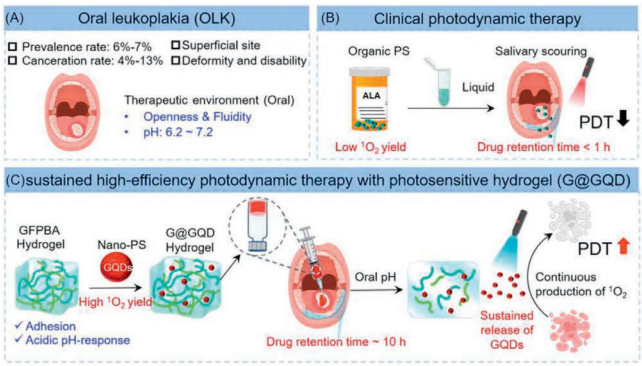
© 2026 Published by Elsevier B.V. on behalf of Chinese Chemical Society and Institute of Materia Medica, Chinese Academy of Medical Sciences.

Oral leukoplakia (OLK) is a common oral potential malignant disorder (OPMD) with a heightened risk of malignant transformation and a canceration rate of >13% (Scheme 1A) [1–3]. Surgical intervention is primary for OLK managing, but scars and function impairments are typically unavoidable, thus adds further psychological burden to patients. Photodynamic therapy (PDT), a minimally invasive treatment modality based on photosensitizer, oxygen and excitation light [4–7], is appealing for OLK treatment [8–12]. Besides, PDT exerts locally and can spar adjacent healthy tissues from the harm one, thus can better prevent the aesthetic and functional integrity of the affected region. However, the open, moist, and highly dynamic microenvironment of the oral pose makes the drug (photosensitizer) retention problematic, thereby significantly challenging the clinical efficacy of PDT (Scheme 1B) [13,14]. Therefore, an oral mucosal-compatible delivery of photosensitizer with long-term drug retention for sustained therapeutic efficiency is highly demanded [15,16].

Supramolecular hydrogels are a typical biocompatible and injectable drug dosage form, which could help to avoid the various adverse consequences of systemic administration and have been widely studied in the field of drug delivery [17–20]. In recent years, natural guanosine (G) and its derivatives have emerged as ideal candidates for the construction and function of supramolecular hydrogels because of the existence of intrinsic hydrogen bond receptor and donor groups, which facilitate the formation of reversible non-covalent interactions and exhibit superior self-assembly capabilities [21,22]. Especially, the diol structure within G is capable of forming a dynamic and reversible borate ester linkage with boric acid, which enables the hydrogel to facilitate a controlled and sustained release of encapsulated drug molecules based on the break of the boryl ester bond [23–26]. The above features suggest that G-based supramolecular self-assembly may provide new opportunities for the construction of oral mucosal photosensitive delivery [27,28].

* Corresponding author.
E-mail address: zhouronghui@scu.edu.cn (R. Zhou).

https://doi.org/10.1016/j.cclet.2025.111282
1001-8417/© 2026 Published by Elsevier B.V. on behalf of Chinese Chemical Society and Institute of Materia Medica, Chinese Academy of Medical Sciences.



Scheme 1. G@GQD photosensitive hydrogel for sustained and high-efficacy PDT of oral leukoplakia.

Herein, a novel photosensitive G-based hydrogel system (G@GQD) was successfully constructed by a one-pot method, in which the graphene quantum dots (GQDs) with highly photosensitive activity was loaded through three dimensional (3D) fiber network physical encapsulation (Scheme 1C). Firstly, because of their adhesive and acidic pH-responsive characteristics, G@GQD hydrogel can be well suited for enhancing the retention time of GQDs in the oral cavity. In addition, our previous study demonstrated that GQDs exhibit superior efficiency in PDT due to their higher singlet oxygen yield when compared with organic photosensitizer that approved for clinical use [29]. Thus, the G@GQD hydrogel achieves sustained therapeutic efficiency *in vitro* through continuously releasing GQDs and simultaneously generating high levels of reactive oxygen species (ROS). At the same time, *in vivo* studies using 4-nitroquinoline-1-oxide (4-NQO)-induced OLK mouse models revealed that G@GQD-mediated PDT significantly enhances therapeutic efficacy with long-term drug retention.

To implement the proposed GQDs loading process, GQDs with a size of 13.2 ± 2.7 nm were first prepared by hydrothermal method according to the literature previously reported (Fig. S1 in Supporting information) [30], which possesses a wide absorption at 400–600 nm as well as a red fluorescence emission at ~665 nm [31]. Building on our previous development of hydrogels with good adhesion properties that incorporate 2-formylphenylboronic acid (2-FPBA) and G [32], the proposed photosensitive hydrogel system (abbreviated as G@GQD) was engineered through a straightforward one-pot synthesis involving G, 2-FPBA and GQDs. Meanwhile, the hydrogel without GQDs (abbreviated as GFPBA) was also fabricated at the same time. As shown in Fig. 1A, both the GFPBA and G@GQD demonstrated superior gelation stability, retaining their structure without collapse even after 14 days, confirming successful preparation of the G@GQD hydrogel. Meanwhile, fluorescence and UV absorption characterization indicate that GQDs has been successfully incorporated into the hydrogel matrix (Figs. 1B and C), and the optimal concentration of GQDs for loading was determined through fluorescence intensity measurements (Fig. S2 in Supporting information). Furthermore, after embedding GQDs, the zeta potential of the photosensitive hydrogel G@GQD shifted from −36.9 mV (GFPBA) to −28.2 mV, indicating successful incorporation of the positively charged GQDs (+27.8 mV) through electrostatic interactions, thus forming the G@GQD hydrogel (Fig. 1D). Finally, the fiber networks of G@GQD exhibit bright dotted protrusions compared to GFPBA from the morphologies characterized by atomic force microscopy (AFM) (Figs. 1E–G), indicating that GQDs were effectively embedded in the 3D fibrous network space of GFPBA.

Then, the supramolecular self-assembly behavior of the G@GQD was characterized by comparing their core self-assembly structure content with that of the GFPBA. As shown in Fig. S3 (Supporting information), the presence of hydrogen bonds is confirmed

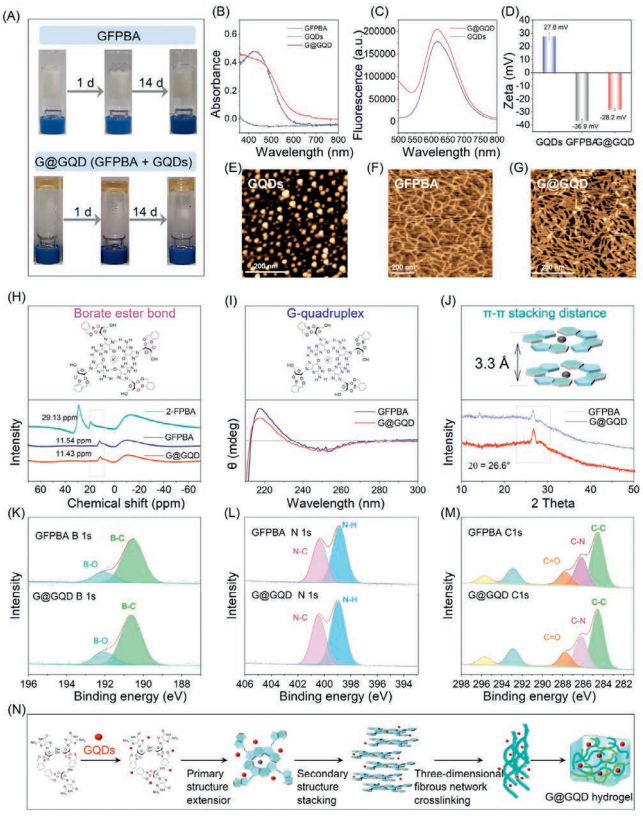


Fig. 1. Preparation and characterization of the G@GQD hydrogel. (A) The vial tube inversion of GFPBA and G@GQD hydrogels (concentration of GQDs in hydrogels: 1.8 μmol/L). (B) Ultraviolet-visible (UV–vis) spectroscopy of GQDs, GFPBA and G@GQD. (C) Fluorescence spectra of GQDs and G@GQD at excitation wavelengths of 450 nm. (D) Zeta potential of GQDs, GFPBA and G@GQD. Data are presented as mean ± standard deviation (SD) ($n = 3$). (E–G) AFM images of GQDs, GFPBA and G@GQD. Scale bar: 200 nm. (H) ^{11}B-NMR of 2-FPBA, GFPBA and G@GQD (I) CD spectral data of GFPBA and G@GQD. (J) XRD patterns of GFPBA and G@GQD. (K–M) XPS data for N, C, and B elements of GFPBA and G@GQD. (N) Schematic diagram of the self-assembly behavior and loading mechanism of GQDs in the G@GQD hydrogel.

by the disappearance of the ν_{O-H} (3350–3067 cm^{-1}) peak in the Fourier transform infrared spectroscopy (FTIR) spectra. Meanwhile, boron nuclear magnetic resonance (^{11}B-NMR) [33,34] further captured the boronate ester bonds of GFPBA (11.54 ppm) and G@GQD (11.43 ppm), while the arylboronic acid structure from 2-FPBA (29.93 ppm) was not detected (Fig. 1H). Subsequently, circular dichroism (CD) shows that G@GQD and GFPBA have a negative peak at 252 nm and a positive peak at 218 nm (Fig. 1I), indicating that the stacked G-quartet heads are in a head-to-head stacking manner [35,36]. The fluorescence enhancement experiment of thioflavin T (ThT) confirmed the relevant existence of G-quadruplexes (Fig. S4 in Supporting information). X-ray diffraction (XRD) also clearly showed the presence of 3.36 and 3.35 Å structures in the hydrogel (Fig. 1J and Fig. S5 in Supporting information), which are characteristic π-π stacking distances [37,38]. To further investigate the loading mechanism of GQDs within the G@GQD, X-ray photoelectron spectroscopy (XPS) was examined in Figs. 1K–M. The analysis revealed that the N, C, and B elementals in G@GQD remained unchanged relative to GFPBA, indicating no new chemical bonds formed. Consequently, it is evident that the fundamental supramolecular self-assembly behaviour of the G@GQD closely resembles that of the GFPBA. The guanine bases self-assemble into G-tetramers through hydrogen bonding, while the *o*-diol groups in the ribose of guanine react with boric acid from 2-FPBA to create borate, resulting in the formation of a "G-tetramer-boric acid" structure, simultaneously GQDs is physically

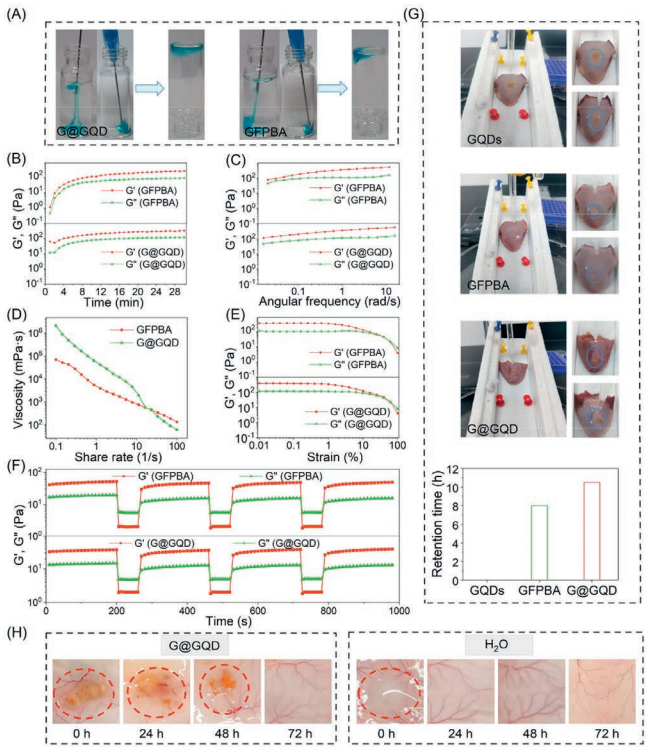


Fig. 2. Mechanical and adhesion properties of G@GQD hydrogel: (A) Visual injection experiment of methyl blue by GFPBA and G@GQD. (B) Time scan of GFPBA and G@GQD hydrogels within 30 min. (C) Frequency scanning of GFPBA and G@GQD hydrogels. (D) Test the viscosity of GFPBA and G@GQD hydrogels at the shear rate of 0.1–100 s^{-1}. (E) Strain scanning test GFPBA and G@GQD hydrogels GFPBA and G@GQD at a constant frequency of 1 Hz. (F) The self-healing ability of GFPBA and G@GQD hydrogels was tested under 0.1 % and 100 % stress, repeated for three times. (G) GQDs, GFPBA and G@GQD hydrogels were coated on pig tongue and washed at the flow rate of PBS (1 mL/min), and the residence time histogram of GQDs, GFPBA and G@GQD on pig tongue surface was also obtained. (H) G@GQD hydrogel (20 μL) and H_2O were injected subcutaneously and degradation was observed at specific time points (0, 24, 48 and 72 h).

encapsulated. This structure then proceeds to engage in longitudinal π-π stacking interactions, which subsequently twist into a fibrous network, ultimately culminating in gelation, as depicted in Fig. 1N.

Dynamically covalently cross-linked hydrogels are typically injectable and can achieve minimally invasive drug delivery [39,40], so the mechanical properties of the G@GQD hydrogel were then validated to assess their potential for injectable drug delivery. As shown in Fig. 2A, the methyl blue visualization injection experiment verified the injectability of both the G@GQD and GFPBA hydrogels as they could be injected through the syringe and quickly gelatinized *in situ* again. Rheological experiments further quantitatively analyzed the shear-thinning and self-healing properties of hydrogels. Time and frequency scans showed that both GFPBA and G@GQD possess solid-like properties ($G' > G''$) and can rapidly gelate within 5 min (Figs. 2B and C). Viscosity scanning indicated that the GFPBA and G@GQD have shear-thinning properties (Fig. 2D), and strain scanning further shown that both GFPBA and G@GQD hydrogels can achieve a "gel-solution" transition when the applied strain reaches 67 % (Fig. 2E). Self-healing scan results revealed that the GFPBA and G@GQD hydrogels almost unaffectedly maintain their storage modulus after undergoing three "gel-sol-gel" transitions (Fig. 2F). The above experiments provide compelling evidence of the excellent injectability and self-healing properties of G@GQD. Importantly, the incorporation of GQDs does not compromise these properties, which is crucial for their potential as an effective local drug delivery system for PDT treatment of OLK.

To further explore the adhesion properties of G@GQD hydrogel, the flow method experiment demonstrated that the G@GQD hydrogel significantly increased its retention time on the pig tongue to 10.5 h, compared to GQDs alone (Fig. 2G). Furthermore, the subcutaneous degradation time in Kunming (KM) mice showed that both G@GQD hydrogel could be rapidly *in-situ* formed on the back of mice after injection, and completely degraded within approximately 3 days. The H_2O solution (as the control group) was completely cleared within 1 day after injection (Fig. 2H). The improved adhesive properties significantly prolong the residence time of the liquid photosensitizer at the oral lesion, thereby validating the local drug delivery potential of G@GQD for OLK-PDT treatment.

After clarifying the loading mechanism of GQDs in the G@GQD hydrogel, the drug release behavior of the G@GQD hydrogel was further explored. Significantly, research has revealed that borate ester bond possesses an acidic pH-responsive property, allowing it to potentially undergo reversible bond cleavage at weakly acidic pH levels [41,42]. The feature triggers G@GQD degradation at pH levels below the pK_a of 2-FPBA (7.65–8.71), leading to the release of encapsulated GQDs. Base on this, we placed the G@GQD in phosphate-buffered saline (PBS) buffer solutions with different pH values (5.4, 6.4, 7.4) to simulate and evaluate the sustained release of GQDs under weakly acidic oral conditions. Observations and fluorescence measurements were conducted at subsequent time points to calculate the cumulative release of GQDs. The study showed that the G@GQD hydrogel exhibited significant pH-responsiveness, with hydrogel disintegration rates increasing as the pH level decreased (Fig. 3A). Specifically, at 72 h, the cumulative release of GQDs reached approximately 90 % in a buffer solution at pH 5.4, around 49 % at pH 6.4, and roughly 28 % at pH 7.4 (Fig. 3B).

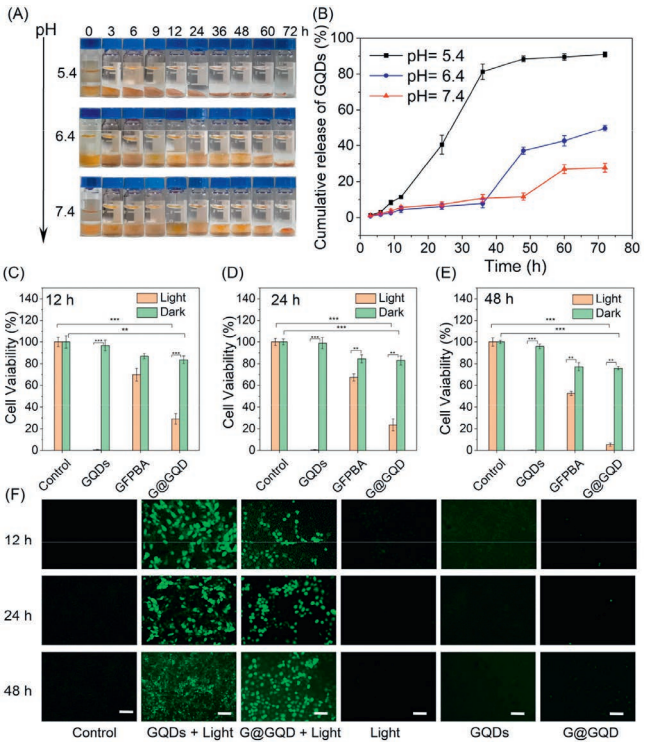


Fig. 3. Sustained PDT effects of G@GQD hydrogel *in vitro*. (A) Sustained release images of G@GQD hydrogel. (B) Sustained-release profile of GQDs from the G@GQD hydrogel. (C–E) CCK-8 assessment of cytotoxicity: GQDs, GFPBA and G@GQD (200 nmol/L) and DOK cells incubated at different times (12, 24, 48 h) under white light (1.0 W/cm^2) irradiation for 5 min. (F) DCFH-DA probe for imaging of ROS generation assessment in DOK cells after treatment with GQDs, GFPBA and G@GQD at different times. Scale bar: 100 μm. Data are presented as mean ± SD ($n = 3$). $^{**}P < 0.01$, $^{***}P < 0.001$.

Then, the release data of GQDs from G@GQD was analyzed using four mathematical models to determine their release mechanism [43]. The results indicated that the release kinetics of GQDs from the G@GQD closely followed the Ritger-Peppas model, which implies that the GQDs' release is primarily attributed to the diffusion and degradation of the hydrogel matrix (Table S5 in Supporting information). This behavior is likely due to the loading mechanism of GQDs, where GQDs is physically embedded within the fiber network. Meanwhile, it was also found that the presence of mucin and lysozyme did not affect the degradation of G@GQD hydrogels (Fig. S6 in Supporting information). To further verify the pH responsiveness of the G@GQD hydrogel, we prepared hydrogel in buffer solutions with varying pH levels. As shown in Fig. S7 (Supporting information), the frequency scan reveals that the strength of the hydrogel under acidic conditions is weaker than that under neutral conditions, implying phenylboronate ester bond is more likely to break in an acidic environment. Meanwhile, the CD results showed that the positive peak at 212 nm of the GFPBA and G@GQD hydrogels at pH 7.4 is stronger than pH 6.4 and 5.4 (Fig. S8 in Supporting information), suggesting the hydrogel are more stable in an alkaline due to the higher content of G-quadruplex structures. In addition, the characteristic absorption peak of oxidized TMB (oxTMB) at 652 nm intensified with increasing GQDs release time (Fig. S9 in Supporting information). This observation further proving that the G@GQD hydrogel has successfully achieved sustained release of GQDs, which will maintain the effective concentrations of GQDs at the OLK lesion, so as to achieve a better PDT therapeutic effect.

Herein, the potential of G@GQD hydrogel for continuous generation of ROS as well as high efficiency PDT *in vitro* were subsequently evaluated. Firstly, the photosensitive oxidation activity of GQDs was verified to ensure an ideal PDT effect in OLK. As seen in Fig. S10A (Supporting information), the phosphorescence characteristic peak of $^1O_2$ from GQDs was observed upon excitation at 450 nm. In addition, electron paramagnetic resonance (EPR) test results provided further evidence that GQDs can produce $^1O_2$ upon irradiation, as evidenced by the observation of the characteristic $^1O_2$ peak induced by 2,2,6,6-tetramethylpiperidine (Fig. S10B in Supporting information). Besides, using DPBF as a singlet oxygen indicator probe [44], Fig. S10C (Supporting information) illustrates that as the illumination time increases, the absorption peak at 420 nm diminishes gradually, indicating the superior $^1O_2$ generation capability of GQDs. To further highlight the superior photodynamic performance of GQDs, their photocytotoxicity was assessed and compared with that of chlorin e6 and protoporphyrin IX (Ce6 and PpIX, Food and Drug Administration-approved photosensitizers) in DOK cells. As shown in Fig. S11A (Supporting information), GQDs have negligible impact on the viability of DOK cells in the absence of light, but upon irradiation, a survival rate of 10 % is achieved when the GQDs concentration is raised to 100 nmol/L. In contrast, as depicted in Fig. S11B (Supporting information), compared to Ce6 and PpIX, a lower concentration of GQDs was able to induce a higher number of apoptotic cells, further confirmed the superior PDT efficacy of GQDs over organic photosensitizers [45]. These results collectively demonstrated that GQDs have an outstanding ability to generate $^1O_2$, which is highly significant for the subsequent *in vivo* PDT of OLK using G@GQD hydrogel.

Then, to study the sustained PDT effect *in vitro*, G@GQD hydrogel was placed in transwell chamber and co-cultured with DOK cells for different periods, where GQDs and GFPBA hydrogel also employed as control. Cell counting kit-8 (CCK-8) assay results showed that GQDs-PDT achieves high cytotoxicity within 12 h, as there is no sustained-release mechanism involved. In the case of G@GQD-PDT, the survival rate of DOK cells progressively diminished from 29 % to 5.3 % over the incubation period extending from 12 h to 48 h (Figs. 3C–E), suggesting a sustained and prolonged PDT effect. Similarly, the same trend in ROS content changes was observed during this process (Fig. 3F). Besides, after 48 h co-cultured, the staining results of live and dead cells [46] showed that more dead cells could be observed in G@GQD-PDT (Fig. S12 in Supporting information), further demonstrating that the sustained PDT of G@GQD hydrogel is effectively realized through sustained releasing GQDs.

Given the promising *in vitro* results of G@GQD hydrogel on OLK cells, further investigation was conducted to evaluate its PDT performance *in vivo*. Initially, hematoxylin and eosin (H&E) staining showed that there was almost no obvious inflammation, edema, congestion, or other adverse phenomena in the skin and major organs of the mice throughout the study period (Figs. S13A and B in Supporting information). The favorable biocompatibility of the G@GQD hydrogel is essential for achieving an effective *in vivo* PDT response in OLK.

To confirm the potential of G@GQD-PDT for the treatment of OLK *in vivo*, we established a mouse tongue OLK model using 4-NQO [47]. All animal experiments were conducted in accordance with the guidelines of the Laboratory Animal Care Principles (NIH) and approved by the Animal Care and Use Committee of West China Stomatological Hospital (No. WCHSIRB-2023–448). The successful establishment of the OLK model was confirmed by a clinical and pathological comparison between wild-type and OLK model mice (Fig. S14 in Supporting information). Subsequently, 32 male mice with white spots on the back of the tongue were selected for PDT and randomly divided into 8 groups for follow-up treatment. As shown in Fig. 4A, firstly, G@GQD hydrogel (20 μL, concentration of GQDs: 1.8 μmol/L), GQDs (20 μL, 1.8 μmol/L) and GFPBA hydrogel (20 μL) were injected into the oral lesion site of mice, and irradiated with 450 nm laser for 3 min, and repeated once every 7 days, for a total of 3 treatments. Throughout the treatment, lesions in all groups except for the G@GQD hydrogel + light group showed continuous progression, with the OLK area gradually enlarging, hardening, and becoming more prominently protruding from the mucosal surface. In contrast, the G@GQD hydrogel + light group exhibited progressive improvement in the OLK region (Fig. 4B). All mice were killed after 21 days of treatment, and the efficacy was

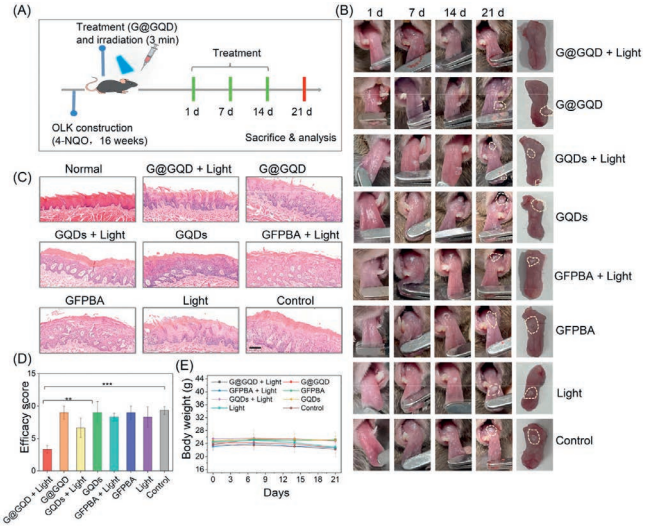


Fig. 4. *In vivo* PDT effect of the G@GQD hydrogel in oral leukoplakia. (A) Schematic diagram of the timeline for the OLK mouse model treated with the G@GQD hydrogel. (B) Pictures of treatment of OLK mice in each group at 1, 7, 14 and 21 days. (C) H&E staining data of tongue sections of OLK mice in each group after treatment. Scale bar: 100 nm. (D) Columnar statistical chart of treatment score effect of OLK mice in each group after PDT. (E) Body weight records of OLK mice in each group at 1, 7, 14 and 21 days. Data are presented as mean ± SD ($n = 4$). $^{**}P < 0.01$, $^{***}P < 0.001$.

judged according to the occurrence of lesions and pathological manifestations [47]. As shown in Fig. 4C, except G@GQD hydrogel + light group and GQDs + light group, all groups displayed evident epithelial dysplasia, indicating an inability to retard or reverse the advancement of OLK. While for GQDs + light group, the degree of epithelial dysplasia was relatively mild due to the unsustainable photodynamic effect. As anticipated, the G@GQD hydrogel + light group demonstrated the highest efficacy and the lowest scoring, with only mild epithelial thickening observed relative to the normal group (Fig. 4D). These results indicate that the G@GQD hydrogel exhibits a potent anti-OLK-PDT effect *in vivo*, aligning with the outcomes of *in vitro* studies. In addition, no significant weight loss was observed in the mice in each group during the entire treatment process (Fig. 4E), and H&E staining (heart, liver, spleen, lung, and kidney) showed no significant pathological changes during each treatment process (Fig. S15 in Supporting information), further reaffirming the satisfactory biocompatibility of G@GQD hydrogel during *in vivo* treatment of OLK.

Subsequently, immunohistochemical (IHC) staining of clinical tissue samples corroborated these findings. Analysis of Ki-67 expression revealed that the G@GQD-PDT treatment group exhibited the lowest number of Ki-67-positive cells (Figs. S16A and B in Supporting information). Terminal deoxynucleotidyl transferase-mediated dUTP nick-end labeling (TUNEL) immunofluorescence assays demonstrated increased green fluorescence following G@GQD hydrogel-mediated PDT, indicating a higher level of apoptosis in DOK cells (Fig. S16C in Supporting information). Meanwhile, the statistical diagram of TUNEL positive cells obviously showed that the G@GQD-PDT group had highest number of apoptotic cells (Fig. S16D in Supporting information). In summary, we have preliminarily revealed that G@GQD hydrogel can achieve high efficiency PDT in OLK model mice by sustained releasing of GQDs, thereby promoting cell apoptosis.

Addressing the challenge of limited PDT performance in OLK due to the drug retention problematic caused by saliva and tongue movement, this study successfully developed an oral mucosal-compatible photosensitive hydrogel (G@GQD) with favorable adhesion *via* a one-pot method. Specifically, the G@GQD hydrogel was constructed by incorporating GQDs into a G-based hydrogel through a 3D fiber network physical encapsulation process, which possesses good biocompatibility, injectable and self-healing properties. Due to its superior adhesive characteristics, the G@GQD hydrogel showed a markedly prolonged retention duration in moist and dynamic oral environments when compared to free GQDs. Leveraging this advantage, GQDs can be sustainably released from G@GQD hydrogel in response to weak acidity, ensuring prolonged drug retention and sustained therapeutic efficacy. Finally, this photosensitive hydrogel system also demonstrated improved efficacy in PDT for 4-NQO-induced OLK lesions in mice, suggesting a promising strategy in overcoming the drug retention barrier for OLK therapy.

Declaration of competing interest

The authors declare that they have no known competing financial interests or personal relationships that could have appeared to influence the work reported in this paper.

CRediT authorship contribution statement

Zhengzheng Lv: Writing – original draft, Methodology, Formal analysis, Data curation. **Xin Xia:** Methodology, Data curation. **Peisheng Cao:** Data curation. **Qi Han:** Data curation. **Hang Zhao:** Project administration, Conceptualization. **Ronghui Zhou:** Writing – review & editing, Methodology, Funding acquisition, Conceptualization. **Peng Wu:** Writing – review & editing, Funding acquisition, Conceptualization.

Acknowledgments

We gratefully acknowledge the financial support from the National Key R&D Program of China (No. 2022YFC2402900 and 2022YFC2402901), the National Natural Science Foundation of China (No. 82373394), the Sichuan Science and Technology Program (No. 2025NSFTD0001), and the Multidisciplinary Research Program of West China Hospital of Stomatology, Sichuan University (No. RD-03–202109). We also would like to thank Dr. Hanjiao Chen and Dr. Yunfei Tian of Analytical & Testing Center, Sichuan University, for their help in EPR and XPS data collection

Supplementary materials

Supplementary material associated with this article can be found, in the online version, at doi:10.1016/j.cclet.2025.111282.

References

[1] S. Petti, Oral Oncol. 39 (2003) 770–780.
[2] S. Warnakulasuriya, A. Ariyawardana, J. Oral Pathol. Med. 45 (2016) 155–166.
[3] M. Lyu, Y. Guo, S. Li, D. Yang, H. Hua, Int. Dent. J. 67 (2017) 252–259.
[4] P. Agostinis, K. Berg, K.A. Cengel, et al., *CA* Cancer J. Clin. 61 (2011) 250–281.
[5] M. Lan, S. Zhao, W. Liu, Adv. Healthc. Mater. 8 (2019) 1900132.
[6] R. Zhou, X. Zeng, H. Zhao, Q. Chen, P. Wu, Coord. Chem. Rev. 452 (2022) 214306.
[7] Z. Gao, X. Zheng, W. Liu, et al., Chin. Chem. Lett. 36 (2025) 109874.
[8] M. Pietruska, S. Sobaniec, P. Bernaczyk, Photodiagn. Photodyn. Ther. 11 (2014) 34–40.
[9] Q. Chen, H. Dan, F. Tang, Int. J. Oral Sci. 11 (2019) 14.
[10] X. Jin, H. Xu, J. Deng, Photodiagn. Photodyn. Ther. 28 (2019) 146–152.
[11] D. Yang, Y. Song, J. Liu, et al., J. Dent. Res. 103 (2024) 1227–1237.
[12] Y. Tao, C. Yan, Y. Wu, Adv. Funct. Mater. 33 (2023) 2303240.
[13] M. Avila, D.M. Ojcius, Ö. Yilmaz, DNA Cell Biol. 28 (2009) 405–411.
[14] C. Cui, L. Mei, D. Wang, Nat. Commun. 14 (2023) 7707.
[15] Y. Wu, Z. Wang, Y. Ge, J. Control. Release 370 (2024) 747–762.
[16] L. Xie, X. Zhang, X. Wang, et al., Chin. Chem. Lett. 36 (2025) 110848.
[17] G. Fang, X. Yang, S. Chen, Coord. Chem. Rev. 454 (2022) 214352.
[18] A.N. Zelikin, C. Ehrhardt, A.M. Healy, Nat. Chem. 8 (2016) 997–1007.
[19] S. Bernhard, M.W. Tibbitt, Adv. Drug Deliv. Rev. 171 (2021) 240–256.
[20] M.J. Webber, R. Langer, Chem. Soc. Rev. 46 (2017) 6600–6620.
[21] J.T. Davis, G.P. Spada, Chem. Soc. Rev. 36 (2007) 296–313.
[22] G.M. Peters, L.P. Skala, T.N. Plank, J. Am. Chem. Soc. 137 (2015) 5819–5827.
[23] R. Nishiyabu, Y. Kubo, T.D. James, J.S. Fossey, Chem. Commun. 47 (2011) 1124–1150.
[24] H. Zhao, H. Feng, J. Liu, Biomaterials 230 (2020) 119598.
[25] X. Xia, S. Song, Y. Wen, Biomater. Sci. 11 (2023) 3092–3103.
[26] J. Qi, T. Ding, T. Liu, Adv. Funct. Mater. 32 (2022) 2204273.
[27] L. Zhang, L. Lei, Z. Zhao, et al., Chin. Chem. Lett. 36 (2025) 110316.
[28] L. Hu, C. Song, H. Li, Macromol. Biosci. 24 (2024) 2200565.
[29] Y. Li, S. Wu, J. Zhang, R. Zhou, X. Cai, Cell Prolif. 53 (2020) e12821.
[30] J. Ge, M. Lan, B. Zhou, Nat. Commun. 5 (2014) 4596.
[31] R. Zhou, X. Lu, Q. Yang, P. Wu, Chin. Chem. Lett. 30 (2019) 1843–1848.
[32] S. Wu, X. Xia, R. Zhou, H. Zhao, Macromolecules 56 (2023) 5813–5824.
[33] H.L.D. Hayes, R. Wei, M. Assante, J. Am. Chem. Soc. 143 (2021) 14814–14826.
[34] G.M. Peters, L.P. Skala, T.N. Plank, J. Am. Chem. Soc. 136 (2014) 12596–12599.
[35] D.M. Gray, J.D. Wen, C.W. Gray, Chirality 20 (2008) 431–440.
[36] S. Masiero, R. Trotta, S. Pieraccini, Org. Biomol. Chem. 8 (2010) 2683–2692.
[37] Y. Li, L. Su, Y. Zhang, Adv. Sci. 9 (2022) 2103485.
[38] K. Matsumura, K. Tateno, Y. Tsuchido, H. Kawai, ChemPlusChem 86 (2021) 1421–1425.
[39] G.D. Cha, W.H. Lee, S.H. Sunwoo, ACS Nano 16 (2022) 554–567.
[40] S. Ran, L. Xue, X. Wei, J. Mater. Chem. B 12 (2024) 6005–6032.
[41] Y. Guan, Y. Zhang, Chem. Soc. Rev. 42 (2013) 8106–8121.
[42] T. Liu, Y. Du, Y. Yan, Mater. Today 62 (2023) 71–97.
[43] X. Wang, O. Ronsin, B. Gravez, Adv. Sci. 8 (2021) 2004213.
[44] M.P. Murphy, H. Bayir, V. Belousov, Nat. Metab. 4 (2022) 651–662.
[45] Q. Ning, Y. Zhang, H. Sun, et al., Chin. Chem. Lett. 36 (2025) 111133.
[46] L. Zhao, J. Li, G. Chen, et al., Chin. Chem. Lett. 37 (2026) 110959.
[47] D. Kanojia, M.M. Vaidya, Oral Oncol. 42 (2006) 655–667.